THE ASTROPHYSICAL JOURNAL, 405:312–326, 1993 March 1

A SPECTROSCOPIC STUDY OF THE SHORT-PERIOD ECLIPSING WOLF-RAYET BINARY CX CEPHEI (WN5+O5 V)

DAVID LEWIS,[1] ANTHONY F. J. MOFFAT, JAYMIE M. MATTHEWS, CARMELLE ROBERT,[2] AND SERGEY V. MARCHENKO[3]
Département de Physique, Université de Montréal C.P. 6128, Succursale A, Montréal, Québec, Canada H3C 3J7; and Observatorie du Mont Mégantic
Received 1992 July 24; accepted 1992 September 3

ABSTRACT

We use some 60 blue 5 Å resolution CCD spectra to derive a greatly improved circular velocity orbit for the 2.13 day eclipsing Wolf-Rayet binary CX Cephei. We find $K_O = 240 \pm 8$ m s^{-1} and $K_{WR} = 340 \pm 10$ km s^{-1}, corresponding to masses of $M_O \sin^3 i = 25.2 \pm 1.9\ M_\odot$ and $M_{WR} \sin^3 i = 17.8 \pm 1.4\ M_\odot$. However, reliable mass estimates must await a clear determination of the orbital inclination. The O-type companion is hotter than previously thought: O5 V instead instead of O8 V.

We also find evidence in the velocities of the strong He II λ4686 line for a secondary period at exactly one-third of the orbital period. This is *not* a harmonic resulting from a slight eccentricity of the orbit, but is probably due to a tidal distortion of the envelope where He II λ4686 is emitted.

The unblended emission lines He II λ4686, N IV λ4058, and (slightly blended) N V λ4063 show clear, phase-dependent variations in strength, as does the He I λ3888 P Cygni absorption edge. We present a qualitative model to account for the differing behavior of these lines. The model invokes a bow shock created by the presence of the O star orbiting in the W-R wind, in addition to direct heating of the W-R wind by the O star radiation.

Subject headings: binaries: eclipsing — stars: individual (CX Cep) — stars: Wolf-Rayet

1. INTRODUCTION

There are presently 172 Wolf-Rayet (W-R) stars known in the Galaxy and 123 in the Magellanic Clouds (van der Hucht 1991). Of these, it is estimated that over 43% are members of close W-R + O binary systems (Moffat et al. 1986), of which only a few are eclipsing. These include V444 Cyg, CQ Cep, and CX Cep in the Galaxy and HD 5980 in the SMC.[4] The eclipsing systems are particularly important since they yield information on the geometry of the binary and on fundamental properties of the stars themselves.

CX Cep (=W-R 151) was discovered to be a W-R star by M. E. Walther in 1945 (Vyssotsky, Miller, & Walther 1945) and was subsequently studied by Hiltner (1946, 1948). He established that CX Cep is an eclipsing binary system with shallow eclipses and estimated its period to be $2^d.1267$. It has a mean, out-of-eclipse continuum magnitude and color of $v = 12.37$ and $b-v = 0.65$. It is situated at $l = 102°.66$, $b = +01°.39$ at an estimated distance of 6 kpc (van der Hucht et al. 1988), with an interstellar extinction of $A_v = 4.02$ mag.

Hiltner (1948) found the spectral class of the W-R component to be WN5 and the velocity amplitude of its orbit to be $K_{WR} \simeq 290$ km s^{-1}, based on the strong emission line He II λ4686. Later, Massey & Conti (1981) used one emission (N V λ4058) and five photospheric absorption lines to determine the velocity amplitude ratio of the two components from a small number of spectra. Taking Bracher's (1966) analysis of Hiltner's (1948) data, Massey & Conti adopted $K_{WR} = 300$ km s^{-1}. Then, assuming that the He II λ4686 and N IV λ4048 lines have the same amplitude, they applied their amplitude ratio to derive $K_O = 130$ km s^{-1}. The masses of the components follow as $M_{WR} \sin^3 i = 5.3\ M_\odot$ and $M_O \sin^3 i = 12.2\ M_\odot$, with projected semimajor axes of $a_{WR} \sin i = 12.6\ R_\odot$, and $a_O \sin i = 5.5\ R_\odot$.

Assuming that only the W-R star fills its Roche lobe, Massey & Conti went on to conclude that $i \geq 50°$, but the shallowness of the eclipses suggests that i cannot be much larger than this limit. Therefore, Massey & Conti adopted $i = 50°$ to obtain masses of $M_{WR} = 11.8\ M_\odot$ and $M_O = 27.1\ M_\odot$, and orbital separations of $a_{WR} = 16.4\ R_\odot$ and $a_O = 7.2\ R_\odot$.

While Massey & Conti were able to confirm the spectral type of the W-R star as WN5, they could not specify that of the O companion due to the presence of intense W-R emission lines underlying the weak absorption features. They were only able to constrain the type of the O star to be at least as early as O8, with luminosity class V.

Meanwhile, Lipunova & Cherepashchuk (1982) obtained a new light curve of CX Cep and refined the binary period to $P = 2^d.12687$. By assuming that the O star is of type O8, they applied Svechnikov's (1969) solutions for light curves of detached and eclipsing binaries to derive $R_O = 9.1 \pm 1\ R_\odot$ and $M_O = 22.5 \pm 3\ M_\odot$. These values lead to an inclination of $i = 53°$ and total orbital separation of $a = 22.5 \pm 1\ R_\odot$, from which they obtain $M_{WR} = 9.5 \pm 1.5\ M_\odot$ and $R_{WR} = 4.5 \pm 2.5\ R_\odot$.

Later, the orbital inclination was independently estimated from a study of polarization variations of CX Cep by Schulte-Ladbeck & van der Hucht (1989). Their value of $i = 74° \pm 5°$ (where the error is based on the formula of Aspin, Simmons, &

[1] Current address: Department of Atmospheric and Oceanic Sciences, McGill University, 805 Sherbrooke Street West, Montréal, Québec, Canada H3A 2K6.
[2] Current address: Space Telescope Science Institute, 3700 San Martin Drive, Baltimore, MD 21218.
[3] Current address: Instituto de Astronomia, UNAM, Apartado Postal 70-264, México D.F., 04510 Mexico.
[4] Once claimed to be eclipsing systems, CV Ser and GP Cep have light curves which suggest only single-dip variations in wind transparency, not true (core) eclipses.

Brown 1981) contradicts the results from the depths of eclipses in the light curve.

Existing studies of the system have produced a wide range of estimates of component masses and separations, and little attention has been paid to the potential strong interactions between the winds of the two stars. Therefore, the goals of our current study are: (1) to derive an accurate radial velocity orbit of *both* components of CX Cep, which will be necessary for more reliable masses; and (2) to investigate the effects of the interacting winds emanating from the two hot companions in this system.

2. OBSERVATIONS AND DATA REDUCTION

Spectra of CX Cep were obtained during two observing runs in 1987 August and October at the 1.6 m telescope and Cassegrain spectrograph of the Observatoire du Mont Mégantic. In all, we collected 62 CCD (RCA; 512 × 320 pixels of 30 μm × 30 μm) spectra of the system; 57 of these were of sufficient quality for subsequent analysis. Each spectrum of CX Cep was accompanied by a Cu Ar spectrum for wavelength calibration just before and after the stellar exposure. A series of dome flat-field exposures was also taken either at the start or end of each night, along with a series of bias exposures at night's end.

The CX Cep spectra were typically 1 hr exposures and were obtained with a 300 line mm^{-1} grating yielding a 2 pixel resolution of ~5 Å in the 3600–5000 Å range (roughly the same as the data of Massey & Conti 1981). The signal-to-noise ratio in the continuum is ~100 pixel^{-1} at 4000 Å, increasing to ~200 at 5000 Å. The spectra were processed using IRAF; for more details, see Lewis (1991). A journal of observations is given in Tables 1 and 2 for the first and second runs, respectively. The average spectrum is shown in Figure 1.

The data were also analyzed using IRAF. Radial velocities (RVs) were obtained by both the "centroid" and "peak" methods of the SPLOT routine, while equivalent widths (EWs) were derived from the same routine. The "centroid" technique bisects the line profile; the "peak" method locates the maximum of the profile for emission lines (or the minimum for absorption lines). The analysis was tailored to each line due to varying amounts of blending. The unblended emission lines studied here are relatively intense, so both techniques are suitable to measure RVs. Each line is divided into steps of 10% of its peak value and centroid velocities can then be measured based on the profile only above a given level relative to the continuum.

The relatively unblended absorption lines in our spectra are a different matter. They are situated in the 3700–4000 Å domain of the upper Balmer lines, where the sensitivity of our CCD is quite low and the noise level is comparable to the absorption line depths in any individual spectrum. Therefore, we were unable to specify a true continuum in the region. For this reason, the RVs of the absorption lines were obtained by centroiding only. For completeness, we also attempted to

TABLE 1

JOURNAL OF THE 1987 AUGUST SPECTRA OF CX CEPHEI

HJD 2,440,000+	Integration Time (s)	Epoch[a]	ϕ[a]	Radial Velocity (km s^{-1}) N v λ4603 Emission	Radial Velocity (km s^{-1}) Hγ λ4340 Absorption
7009.6240.....	1800	1202	0.8007	−359.0	55.0
7009.6670.....	3600	1202	0.8209	−328.3	35.8
7009.7632.....	3600	1202	0.8661	−284.0	54.9
7009.8091.....	3600	1202	0.8877	−225.4	52.5
7013.6133.....	3600	1204	0.6762	−283.2	99.5
7014.5850.....	3600	1205	0.1331	233.4	−249.9
7014.6328.....	3600	1205	0.1557	250.1	−327.7
7014.6743.....	3600	1205	0.1752	257.8	−328.5
7014.7119.....	3600	1205	0.1929	280.2	−335.8
7014.7476.....	2700	1205	0.2096	277.5	−364.1
7014.8379.....	3000	1205	0.2521	291.8	−347.1
7016.7510.....	3600	1206	0.1517	191.0	−359.3
7016.8091.....	3600	1206	0.1789	254.0	−338.1
7018.6016.....	3600	1207	0.0217	−50.4	−125.6
7019.5776.....	2815	1207	0.4806	96.1	−17.9
7019.6123.....	1629	1207	0.4969	9.5	−44.4
7019.6465.....	3600	1207	0.5129	15.8	−13.5
7019.6919.....	3600	1207	0.5343	−19.3	−36.6
7019.7646.....	3600	1207	0.5685	−100.3	−12.0
7019.8091.....	3600	1207	0.5894	−163.9	−13.4
7019.8521.....	3132	1207	0.6095	−214.5	−2.8
7020.5786.....	3600	1207	0.9512	−219.4	−8.1
7020.6235.....	3600	1207	0.9723	−178.4	−165.6
7020.6680.....	3600	1207	0.9933	−141.8	−147.2
7020.7134.....	3600	1208	0.0145	−117.4	−94.3
7020.8438.....	3600	1208	0.0760	38.6	−289.4

[a] Epoch and phase from the ephemeris of Lipunova & Cherepashchuk 1982; see text.

TABLE 2

JOURNAL OF THE 1987 OCTOBER SPECTRA OF CX CEPHEI

HJD 2,440,000+	Integration Time (s)	Epoch[a]	ϕ[a]	Radial Velocity (km s^{-1}) N v λ4603 Emission	Radial Velocity (km s^{-1}) Hγ λ4340 Absorption
7074.5371.....	3600	1233	0.3211	326.7	−305.2
7074.5820.....	3600	1233	0.3422	300.4	−262.5
7074.6504.....	3600	1233	0.3745	252.4	−208.2
7074.6914.....	3000	1233	0.3937	215.3	−349.2
7074.7295.....	3000	1233	0.4115	161.8	−208.6
7074.7661.....	3000	1233	0.4289	148.0	−156.3
7074.8071.....	3600	1233	0.4482	111.3	−152.2
7075.5117.....	3600	1233	0.7793	−286.6	112.8
7075.5571.....	3609	1233	0.8007	−292.7	204.7
7075.6035.....	3600	1233	0.8226	−298.6	184.3
7080.5879.....	3000	1236	0.1541	303.0	−263.3
7080.6367.....	3600	1236	0.1772	284.3	−293.8
7080.6821.....	3600	1236	0.1984	349.4	−337.5
7080.7461.....	3600	1236	0.2285	316.0	−323.1
7080.7905.....	3600	1236	0.2494	317.6	−444.5
7080.8521.....	3600	1236	0.2784	382.6	−382.0
7080.8965.....	3600	1236	0.2992	375.4	−274.4
7081.4854.....	3600	1236	0.5898	−83.7	174.3
7081.5332.....	3600	1236	0.6124	−111.5	113.3
7081.5815.....	3600	1236	0.6351	−176.9	120.6
7081.6255.....	3600	1236	0.6559	−212.2	198.1
7082.5103.....	3600	1237	0.0700	123.8	−130.4
7082.5557.....	3600	1237	0.0913	177.7	−148.1
7082.6055.....	3600	1237	0.1147	223.0	−223.6
7082.6436.....	3600	1237	0.1327	264.1	−235.6
7082.6792.....	3600	1237	0.1493	272.6	−199.7
7082.7246.....	3600	1237	0.1706	253.3	−309.8
7082.7563.....	3600	1237	0.1857	277.5	−322.5
7082.7886.....	3600	1237	0.2007	300.1	−353.9
7082.8320.....	3600	1237	0.2212	408.0	−189.8
7082.8726.....	3600	1237	0.2402	457.9	−198.8

[a] Epoch and phase as in Table 1.

measure EWs of these lines, but the results have high uncertainties.

Strong blends of emission and absorption occur in CX Cep—specifically, narrow weak absorption lines superposed on wider, more intense emission features. The RVs of these blended absorption lines were measured by the centroid method, taking the emission profile as a sloping "pseudocontinuum" to be rectified for the measurement. On the other hand, because of the contamination of the absorption line, the RV of the emission line cannot be safely measured by the same method. If the absorption line is weak enough, the peak method can be applied with minimal systematic effect. For these features, EW measurements were rejected: in the case of the emission lines, because of the presence of the absorption; in the case of the absorption lines, because the small uncertainty in the pseudocontinuum level is of the same order as the EW variations themselves.

We also have one instance of blended emission lines: a pair of N v lines at λ4603 and 4619 Å are also blended with the N III triplet lines near 4640 Å. Velocities of the N v lines can be obtained reliably near their peaks. On the other hand, the RV of the N III line can only be measured by its peak, since this is a weak feature seriously blended with both N v λ4619 and He II λ4686. Since both N v lines arise from the same multiplet, they should vary in a similar fashion. Therefore, we measure only the equivalent width variations of N v λ4603 to avoid problems with the N v λ4619/N III blend.

3. RESULTS AND DISCUSSION

3.1. *Spectral Types*

According to Hiltner (1948), Massey & Conti (1981), and van der Hucht et al. (1988), the spectral type of the W-R star is WN5. Our mean spectrum shown in Figure 1, together with the classification criteria for WN stars (e.g., van der Hucht et al. 1981) agree with this: N IV λ4058 $\geq$ N v λ4603; N III λ4640 present but weak. Note, however, that a hotter type (WN4) is also acceptable, as given by van der Hucht et al. (1981).

On the other hand, the spectral type of the O star has not been well specified. The absorption lines necessary for classification are superposed on intense emission lines so that recognizing them, let alone measuring them, is almost impossible on photographic plates. The use of a CCD helps here, because of the linear relation between real and observed flux, and the higher S/N which can be achieved. To improve the S/N even more, we have calculated an average spectrum after shifting each individual one to the same *absorption line* velocity, based on the adopted ephemeris. Despite this increase in S/N for the

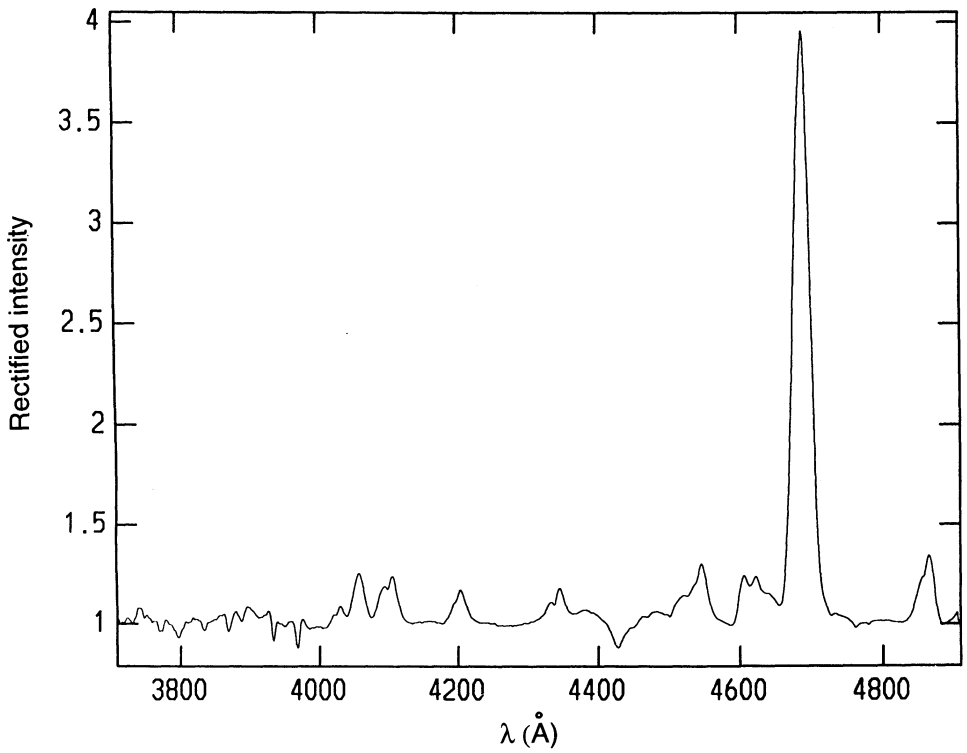

FIG. 1*a*

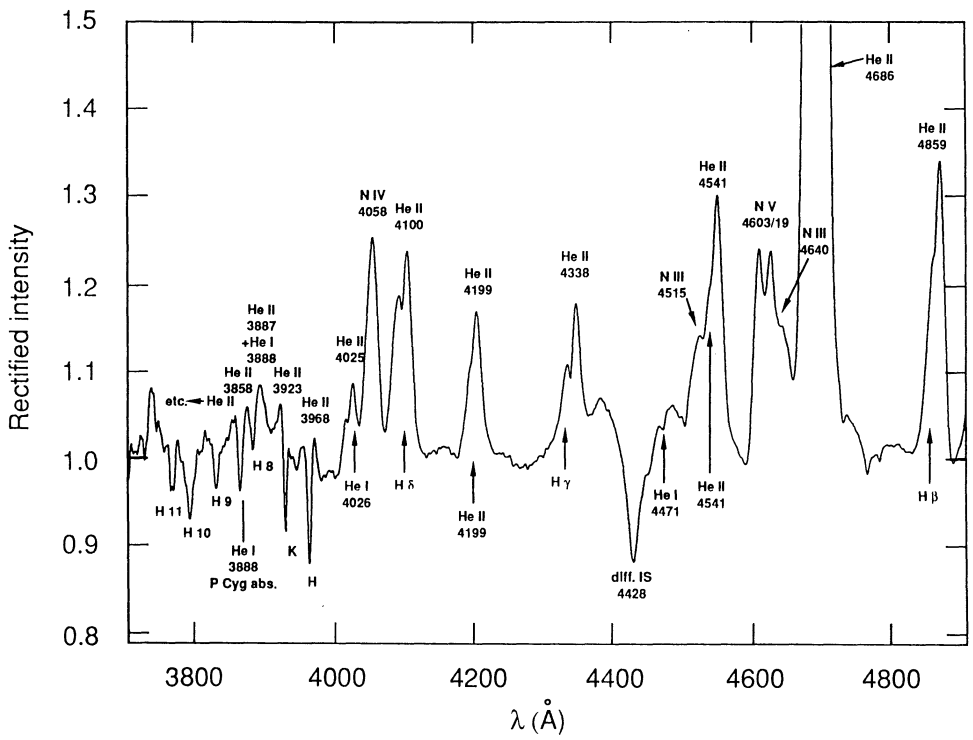

FIG. 1*b*

FIG. 1.—Mean of all 57 spectra of CX Cep, after rectification but no velocity shifting. (*a*) The complete spectrum, (*b*) a magnified view to show the lines which are much weaker than He II λ4686. The major lines are identified.

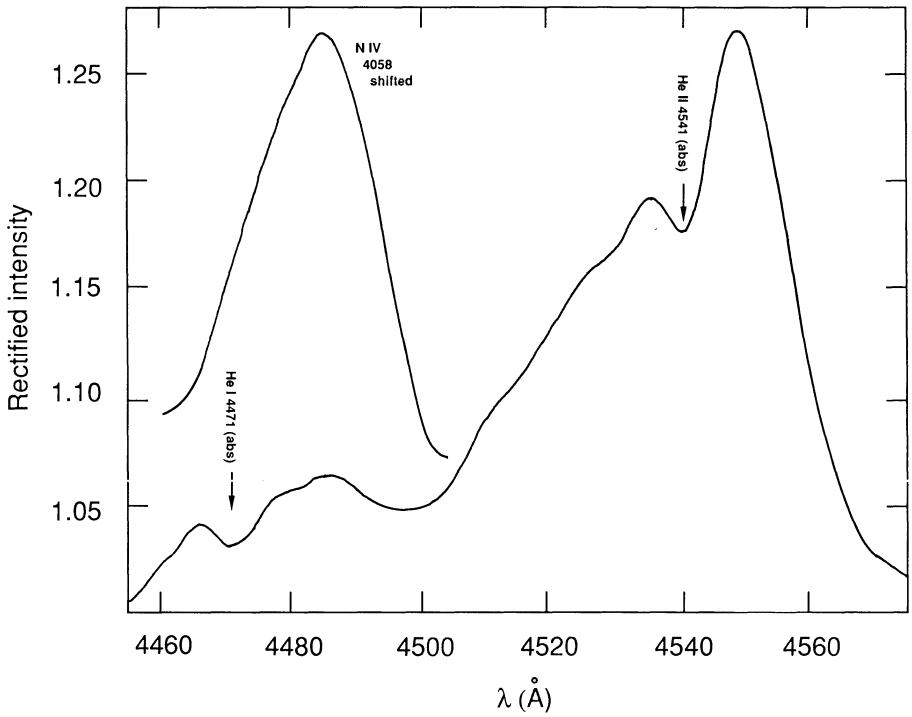

FIG. 2.—A part of the mean spectrum of CX Cep, this time after shifting each individual spectrum to the γ velocity of the absorption-line ephemeris. This considerably deepens the absorption lines without changing their equivalent widths. Clearly evident are the two absorption lines (He I λ4471 and He II λ4541) which are crucial for the spectral classification of O stars. Both lines are superposed on stronger, broader emissions. The mean profile of the pure emission line N IV λ4058 is shown (shifted) for comparison.

O-star absorption lines, the measurements remain difficult because of the uncertain shapes of the underlying emission lines (see Fig. 2).

Nevertheless, we are able to measure from Figure 2 an intensity ratio of He I λ4471/He II λ4542 = 0.33 $\pm$ 0.07. The leads to a spectral type of O5, according to the calibration of Schmidt-Kaler (1982). Later calibrations by Mathys (1988, 1989) yield type O5–O5.5, allowing for the uncertainty in the measured λ4471/λ4542 intensity ratio. In either case, a type of O8 (for which the He I/He II ratio would be 1.3) is clearly excluded.

We can also set a lower bound on the terminal velocity of the W-R wind, based on the blue edge of the absorption component of the He I λ3888 P Cygni profile. We find $v_\infty \simeq 1500$ km s^{-1}. Prinja, Barlow, & Howarth (1990) obtained terminal velocities for the winds of many W-R stars, but not CX Cep, and within a given spectral subtype, there is a wide range of velocities. For the three WN5 stars they studied, they found v_∞ = 1650, 2325, and 3140 km s^{-1}. Unfortunately, this does not place any additional constraints on the spectral type of the W-R star in CX Cep.

3.2. *Orbital Solution*

3.2.1. *RV Curves and Orbital Eccentricity*

To obtain the orbital phases of our observations, we used the ephemeris of primary light minimum from Lipunova & Cherepashchuk (1982):

$$\mathrm{HJD_{min}} = 2444451.4234 + 2.12687\ \mathrm{E}\ .$$

When we fitted general eccentric orbits to the data, we obtain values for the eccentricity of order $e \sim 0.1 \pm 0.1$. In addition, the orientation of periastron was totally different depending on the line used for the velocities. Therefore, we conclude that the eccentricity is $e = 0$. This seems reasonable since most massive (O + O) binaries with periods less than $\sim$30 days have circular orbits (Massey 1981). Moreover, Tassoul's (1987, 1988, 1990) treatment of how tidal effects circularize the orbit of a detached binary lend theoretical support for our conclusion. For massive systems (including W-R + O), he derives a circularization time:

$$t_{\mathrm{circ}} = 400(10^N)^{-1/4} P^{49/12}\ ,$$

where t_{circ} is in years, P is in days, and 10^N (the ratio of macroscopic and microscopic viscosities) is of order 10^4–10^8. For a binary system like CX Cep with a period of $\sim$2 days, $t_{\mathrm{circ}} \simeq 10^2$–$10^3$ yr. This is considerably shorter than the age of the system, since at least 10^6 yr are required for an O star to evolve into a W-R star.

The parameters of the RV orbital fits—amplitude K, systematic velocity γ, and phase at which the line velocity passes through the γ velocity—are given in Tables 3 and 4. The best-defined results are obtained for the N V λ4603 emission line (due to the W-R star) and the Hγ Balmer line (due to the O star). Those velocities are also tabulated in Tables 3 and 4, while the corresponding RV curves for the W-R and O star are shown in Figures 3 and 4, respectively. The residuals from the circular orbital fits to those curves are discussed in § 3.3.

3.2.2. *Velocity Amplitudes*

Usually, lines of higher ionization and lower strength in a W-R wind form closer to the central star, and hence, they reflect smaller RV amplitudes due to the orbital motion (Abbott & Conti 1987).[5] The weakest emission lines with the

[5] This is not always true. For example, Drissen et al. (1986) found that in the case of HD 197406, the RV amplitude of the orbital curve measured for He II λ4686 is *smaller* than that of N IV λ4058.

TABLE 3

RESULTS OF CIRCULAR ORBIT RV FITS TO ALL OBSERVED LINES IN THE RANGE 3700–4600 Å

Line	λ_0 (Å)	Type of Measurement	Level	K (km s^{-1})	γ (km s^{-1})	Phase of γ Crossover	Type of Line
H9	3835.386	Correlation	...	227 ± 25	−21.1 ± 0.4	0.48 ± 0.02	Absorption
H9+H10	...	Correlation	...	179 ± 19	−29.8 ± 0.4	0.49 ± 0.02	Absorption
He I	3888.646	Centroid	...	44 ± 18	−1492.0 ± 0.0	0.18 ± 0.05	Absorption
H8	3889.051	Centroid	...	242 ± 16	−58.1 ± 0.2	0.53 ± 0.01	Absorption
N IV	4057.80	Centroid	0.2	327 ± 10	−123.9 ± 0.1	+0.009 ± 0.005	Emission
N IV	...	Centroid	0.3	327 ± 11	−124.9 ± 0.1	+0.006 ± 0.005	Emission
N IV	...	Centroid	0.4	326 ± 11	−125.6 ± 0.1	+0.003 ± 0.006	Emission
N IV	...	Centroid	0.5	326 ± 12	−129.4 ± 0.2	−0.002 ± 0.006	Emission
N IV	...	Centroid	0.6	323 ± 13	−128.9 ± 0.2	−0.005 ± 0.007	Emission
N IV	...	Centroid	0.7	320 ± 14	−128.0 ± 0.2	−0.009 ± 0.008	Emission
N IV	...	Centroid	0.8	320 ± 16	−127.3 ± 0.2	−0.016 ± 0.009	Emission
N IV	...	Centroid	0.9	317 ± 19	−118.1 ± 0.2	−0.027 ± 0.011	Emission
N IV	...	Peak	...	306 ± 22	−114.1 ± 0.3	−0.026 ± 0.013	Emission
Hδ	4101.737	Centroid	...	230 ± 12	−80.0 ± 0.2	0.49 ± 0.01	Absorption
He II	4199.83	Centroid	...	291 ± 23	+10.1 ± 0.3	+0.45 ± 0.02	Absorption
He II	...	Peak	...	409 ± 14	+16.3 ± 0.2	−0.04 ± 0.01	Emission
Hγ	4340.468	Centroid	...	236 ± 12	−87.2 ± 0.2	0.48 ± 0.01	Absorption
He II	4541.59	Centroid	...	215 ± 14	−55.0 ± 0.2	+0.49 ± 0.01	Absorption
He II	...	Peak	...	405 ± 14	+24.5 ± 0.2	−0.04 ± 0.01	Emission

highest level of ionization should be less affected by tidal distortions and hence should best represent the true orbital motions of the W-R star.

In the case of our spectra, the N V λλ4603, 4619 doublet is the best candidate. The λ4603 line is preferred over λ4619 because of the latter's blend with the N III triplet. For N V λ4603, we obtain $K_{WR} = 340 \pm 10$ km s^{-1}. The N III λ4640 and N IV λ4058 lines give results consistent with this value, as does the He II λ4686 line (except for the strongly asymmetric wings at levels below 50% of the line peak; see Figure 5 and the discussion in § 3.5).

The problem of varying RV amplitude with ionization level does not exist for the O star, whose visible absorption lines are all formed in its photosphere. As expected, therefore, most of

TABLE 4

RESULTS OF CIRCULAR ORBIT RV FITS TO ALL OBSERVED LINES IN THE RANGE 4600–4900 Å

Line	λ_0 (Å)	Type of Measurement	Level	K (km s^{-1})	γ (km s^{-1})	Phase of γ Crossover	Type of Line
N V	4603.2	Centroid	0.7	340 ± 0.1	−2.3 ± 0.1	0.026 ± 0.004	Emission
N V	...	Centroid	0.8	339 ± 9	−3.0 ± 0.1	0.026 ± 0.004	Emission
N V	...	Centroid	0.9	338 ± 10	−0.7 ± 0.1	0.026 ± 0.005	Emission
N V	...	Peak	...	338 ± 10	−9.4 ± 0.1	0.026 ± 0.005	Emission
N V	4619.4	Centroid	0.8	317 ± 8	15.4 ± 0.1	0.033 ± 0.004	Emission
N V	...	Centroid	0.9	316 ± 9	14.8 ± 0.1	0.032 ± 0.004	Emission
N V	...	Peak	...	318 ± 10	7.5 ± 0.1	0.032 ± 0.005	Emission
N III	4641.90	Centroid	...	348 ± 15	−101.6 ± 0.1	−0.09 ± 0.01	Emission
He II	4685.682	Centroid	0.1	306 ± 7	66.9 ± 0.1	+0.021 ± 0.004	Emission
He II	...	Centroid	0.2	317 ± 7	66.1 ± 0.1	+0.013 ± 0.004	Emission
He II	...	Centroid	0.3	327 ± 8	69.1 ± 0.1	+0.005 ± 0.004	Emission
He II	...	Centroid	0.4	336 ± 8	69.4 ± 0.1	−0.002 ± 0.004	Emission
He II	...	Centroid	0.5	343 ± 8	68.3 ± 0.1	−0.009 ± 0.004	Emission
He II	...	Centroid	0.6	347 ± 8	65.8 ± 0.1	−0.015 ± 0.004	Emission
He II	...	Centroid	0.7	349 ± 9	62.1 ± 0.1	−0.021 ± 0.004	Emission
He II	...	Centroid	0.8	349 ± 9	59.2 ± 0.1	−0.026 ± 0.005	Emission
He II	...	Centroid	0.9	345 ± 9	57.8 ± 0.1	−0.030 ± 0.005	Emission
He II	...	Peak	...	344 ± 10	50.0 ± 0.1	−0.030 ± 0.005	Emission
He II	...	Correlation	...	308 ± 7	129.8 ± 0.1	−0.016 ± 0.004	Emission
He II	4859.323	Peak	...	406 ± 13	+44.1 ± 0.1	0.38 ± 0.01	Emission
Hβ	4861.332	Centroid	...	259 ± 11	−132.2 ± 0.2	0.46 ± 0.01	Absorption

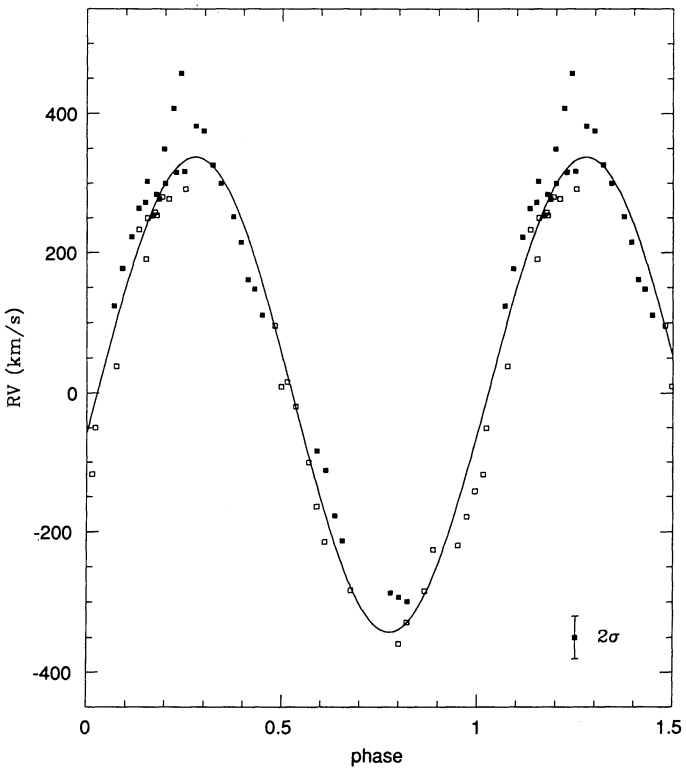

FIG. 3.—The radial velocities of N v λ4603 plotted according to orbital phase as in § 3.2.1. (*Open squares* refer to the 1987 August data, *filled squares* to the 1987 October run.) *Solid curve* is the circular orbital solution to the data.

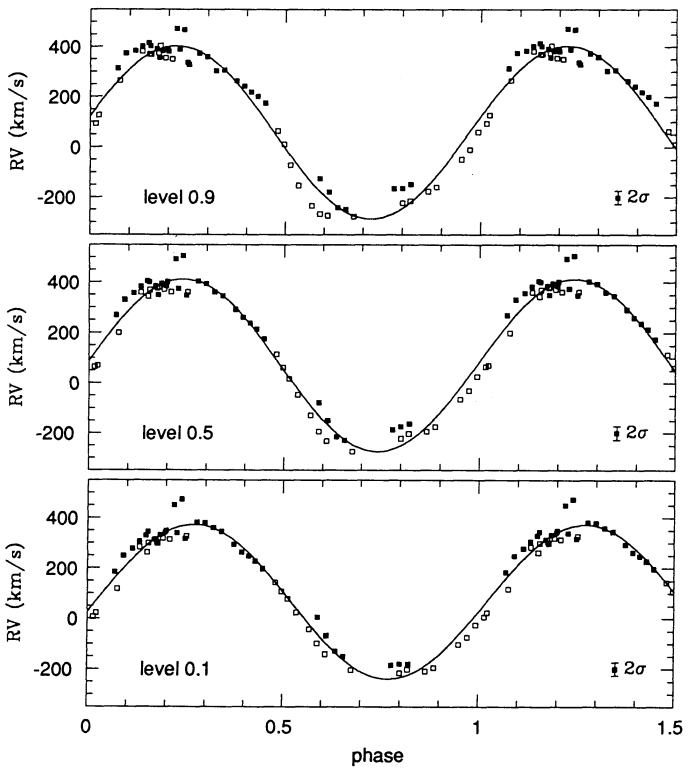

FIG. 5.—Velocities of the He II λ4686 emission line, measured using different parts of the profile. Level 0.9 means that only the upper 10% of the line was measured; level 0.5, the upper 50%; and level 0.1, the upper 90%. Note that the fit to the level 0.1 velocities has a lower amplitude and a different phase. Symbols as in Fig. 3.

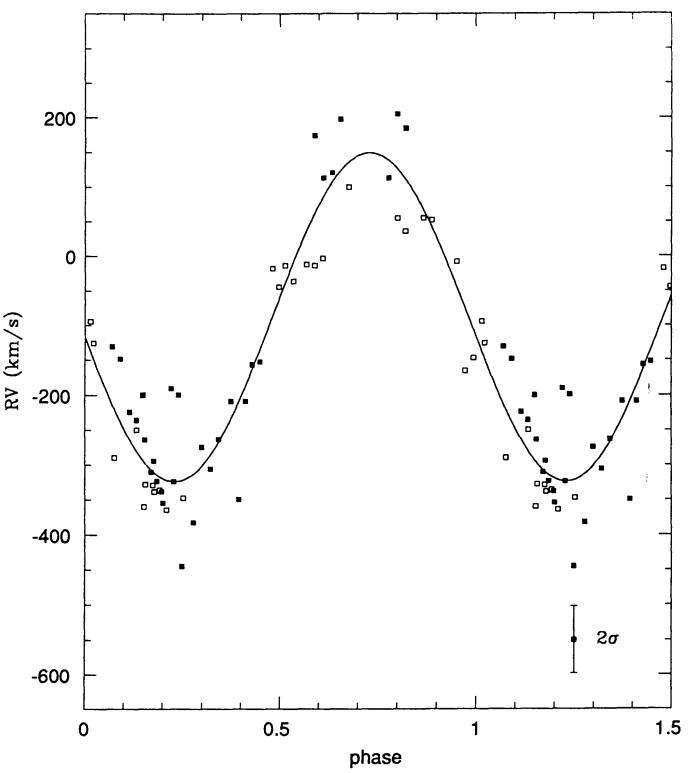

FIG. 4.—Same as Fig. 3, but for the absorption line Hγ λ4340

the O-star lines give self-consistent results. However, the He II Pickering lines are a notable exception, yielding erratic results in both absorption and emission (see Tables 3 and 4). Although there may be a physical explanation for this, we suspect that the blending of emission and absorption lines is a major factor in the uncertain measurements. Fortunately, this is a less serious problem for the hydrogen Balmer lines, whose absorption components from the O star are stronger and better defined. (An exception may be H10, which appears anomalously deep, suggesting a possible blend.) Therefore, we use all the absorption lines except He I λ3888, which is the blue edge of a P Cygni profile and is ascribed to the W-R star.[6] When an unweighted mean of all lines is taken, we obtain $K_O = 243 \pm 6$ km s^{-1}. If the Pickering lines are excluded, the result becomes $K_O = 239 \pm 8$ km s^{-1}, the same within the errors.

We finally adopt $K_{WR} = 340 \pm 10$ m s^{-1} (based on N v λ4603) and $K_O = 240 \pm 8$ km s^{-1} (based on an average of the absorption line results). The total amplitude for the system is thus $K = 580 \pm 13$ km s^{-1}. If we compare our results to those of other authors, we find that our value of K_{WR} is marginally higher, while our value of K_O is significantly higher than Massey & Conti's (1981) value of 130 km s^{-1}. This large difference is possibly due to their small number of spectra, particularly the poor sampling near orbital phases 0.25 and 0.75,

[6] The amplitude of the velocity curve due to this feature is much lower than any other line. This is because this low-energy, metastable He I line is formed relatively far from the W-R star in a region of low wind density, enveloping the orbits of both stars.

where the RVs of the two components have their largest difference.

3.2.3. *Phase Shifts in RV Curves*

The lines which best represent the circular orbit of the system must be those whose velocities pass through the systemic γ velocity close to phase 0.0 for the W-R star and 0.5 for the O star. Note that the γ velocity of the emission lines differs from that of the absorption lines (see Tables 3 and 4), the latter being more representative of the motion of the binary barycenter (Abbott & Conti 1987). The difference arises from the fact that the emission lines form in the expanding wind of the W-R star while the absorption lines form in the O star's photosphere. Nevertheless, the emission and absorption lines move roughly in antiphase (as expected) except for the absorption component of He I λ3888, which is associated with the W-R star.

Allowing for these factors, we still note that the RV curves for various lines pass through their corresponding γ velocities at slightly different orbital phases. These small phase shifts ($\Delta\phi \leq 0.04$) and their variations with level within the line (see Figs. 6 and 7) are not well understood. They may be due to the detailed interactions of the two stellar winds in CX Cep. They are probably not due to small wind perturbations as observed in most W-R stars (Robert 1992), since such effects tend to be random in nature.

3.2.4. *Masses, Radii, and Orbital Inclination*

From Kepler's Laws and our new values of the velocity amplitudes (see § 3.2.2), we obtain

$$M_{\rm O} \sin^3 i = 25.3 \pm 1.9\ M_\odot\ , \quad M_{\rm WR} \sin^3 i = 17.8 \pm 1.4\ M_\odot\ .$$

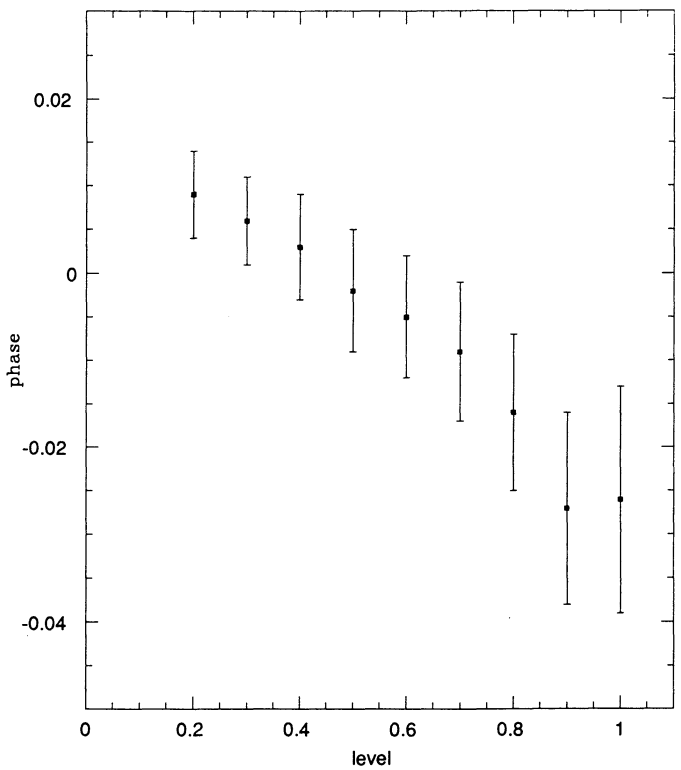

FIG. 6.—Variation of the phase of γ-velocity intercept for the velocity curve of the N IV λ4058 emission line, measured using different parts of the profile. Level 0 corresponds to the entire line, while level 1 corresponds to the line peak.

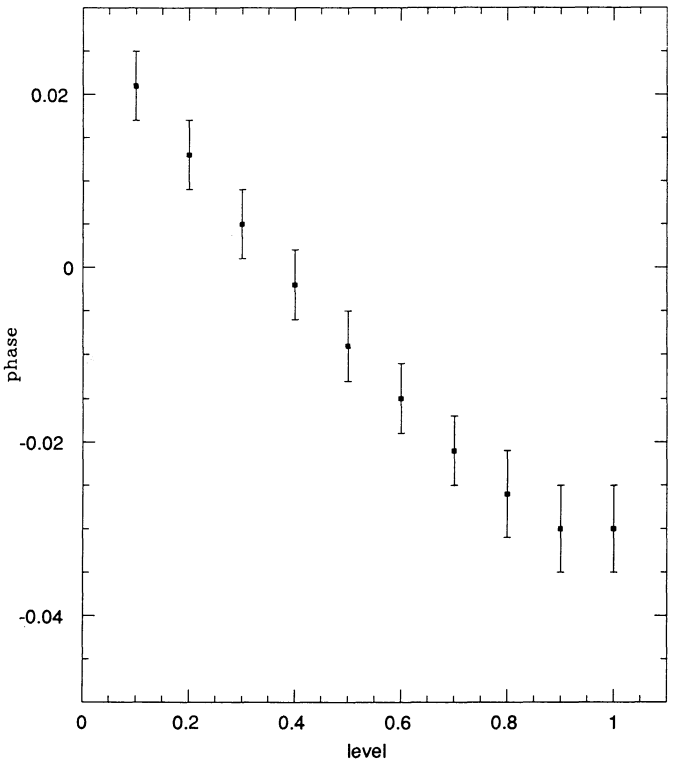

FIG. 7.—Same as Fig. 5, but for the He II λ4686 emission line

The differences from the results of previous authors (§ 1) can be attributed mainly to the differences in $K_{\rm O}$.

If we adopt the inclination $i = 74° \pm 5°$ from the polarimetry of Schulte-Ladbeck & van der Hucht (1989), we derive masses of $M_{\rm O} = 28.4 \pm 6.5\ M_\odot$ and $M_{\rm WR} = 20.0 \pm 4.6\ M_\odot$, and separations of $a_{\rm O} = 10.5 \pm 0.4\ R_\odot$ and $a_{\rm WR} = 14.9 \pm 0.5\ R_\odot$. The semimajor axis of the system is thus $a = 25.4 \pm 0.9\ R_\odot$. According to Lipunova & Cherepashchuk (1982), the radius of the W-R star in CX Cep is $R_{\rm WR} = 4.5 \pm 2.5\ R_\odot$, while Schmidt-Kaler (1982) and Howarth & Prinja (1989) estimate the radius of an O5 V star to be near $12\ R_\odot$. We conclude that, despite its short period, CX Cep is clearly *not* a contact binary.

Following the approaches of Massey & Conti (1981) and Lipunova & Cherepashchuk (1982), we have tried to derive independently the mass of the W-R star and the orbital inclination by adopting a mass for the O star based solely on its spectral type. In the case of early-type stars, empirical masses are scarce, and one is often obliged to use masses based on the theoretical mass-luminosity relation. Harmanec (1988) does provide an estimate of the mass of the O5.5 V star in DH Cep—$M = 52 \pm 12\ M_\odot$—which is consistent with Howarth & Prinja's (1989) value for an O5 V star: $58\ M_\odot$.[7] This latter value yields $i = 49°$ (consistent with that inferred from the light curve but at odds with the polarimetric results) and $M_{\rm WR} = 41\ M_\odot$. The total mass of the system would be $M \sim 100\ M_\odot$ and its semimajor axis would be $a \sim 32\ R_\odot$. This also argues against the system being in contact.

Even so, we prefer inclination and mass estimates based on

[7] A note of caution: Consistency among theoretical masses from other sources (e.g., Schmidt-Kaler's [1982] value of $M_{\rm O5\ V} = 60\ M_\odot$) does not really provide independent support, since all these values rely on the same theoretical assumptions.

direct observation (e.g., polarimetry) rather than those based on models. Not only may such models still tend to overestimate stellar masses, but for any given spectral type, there remains considerable dispersion in the theoretical mass.

3.3. *Search for Secondary Periods*

Velocity variations on time scales much shorter than the orbital period (~a few hours) have been reported in several W-R stars (Vreux 1985; Vreux et al. 1985) and in the W-R binary V444 Cyg (Marchenko 1988a). Such variations might be due to a desynchronization of the star's rotation with respect to the orbital revolution; e.g., when the mass loss of the W-R star exposes deeper—and more rapidly rotating—layers. Desynchronization can also be caused by a difference in the mass-loss rates of both components of a binary. A W-R star will lose mass, and hence angular momentum, at a faster rate than its O companion. If the total angular momentum of the system is conserved, then the synchronization between rotation and orbit is broken.

In fact, we did note small residual variations from our orbital solution (see Figs. 3 and 5) which did not appear completely random. Are there other independent perods present in the CX Cep velocities? Could the orbit be slightly eccentric, introducing harmonic terms which were not included in our circular fit? To answer these questions, we searched for secondary periodicities in the residual RVs (observed minus orbital fit) of several stronger less-blended emission lines: He II λ4686, N IV λ4058 and N V λ4603. The search was conducted by two different approaches: (1) a Fourier periodogram for unequally spaced time series (Matthews & Wehlau 1985; Kurtz 1985) similar to the algorithm of Deeming (1975) but more efficient of computer time; and (2) a "string-length" analysis (e.g., Lafler & Kinman 1965) in which the data are ordered in phase at various trial periods to find curves with the smallest scatter. The second approach has the advantage of allowing an arbitrary *non*sinusoidal shape for any secondary RV curve present in the residuals.

Our preliminary analyses first revealed power at very low frequencies and alias sidelobes extending throughout the frequency range of interest, masking any true signal(s) there. This power is produced by a difference of ~ 50 km s^{-1} (only $\sim 8\%$ of K_{tot} of the orbit) between the means of the two runs which comprise our data. This difference, when combined with the large gap of almost 2 months between the runs, is interpreted by the Fourier routine as a long period. Therefore, to remove this slope in the data, we normalized the velocities in the two runs according to their respective means. There is no way to establish whether this long-term velocity shift is an instrumental drift, an artifact of incomplete sampling of the orbital period during the individual runs, or a genuine stellar variation. However, whatever its source, removal of the straight-line trend from the data does not introduce spurious power at periods less than 2 days.

Note that the centroids of the three lines used for this search have been measured starting from different levels: from 0.1 for He II, 0.2 for N IV, and 0.7 for N V. The results are sensitive to how much of the line is included in the RV determination, and this may be a useful diagnostic of the origin of any secondary periods.

Figure 8*a* shows the Fourier amplitude spectrum of the He II λ4686 residuals. The spectrum is complicated by strong 1 cycle day^{-1} alias peaks, but prewhitening indicates true peaks at one-third, one-sixth, and one-ninth of the orbital period, with

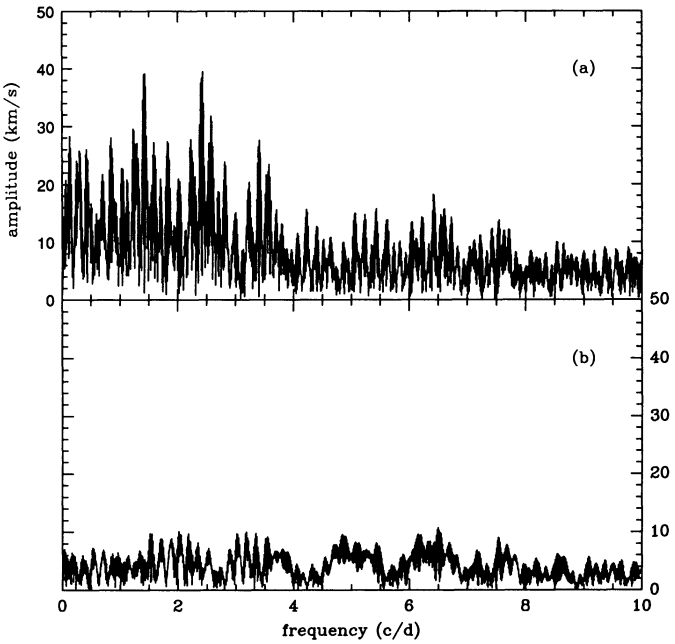

FIG. 8.—(*a*) Fourier amplitude spectrum of the velocity residuals of He II λ4686 (level 0.7) after removal of the circular orbital fit. (*b*) Amplitude spectrum after removing a period of $\frac{1}{3} \times P_{orbit}$ and its first two harmonics.

uncertainties less than $0^d.001$. The principal peak at $\frac{1}{3} \times P_{orbit}$ appears to be significant at above the 99% level, according to Scargle's (1982) "false alarm probability." When a period of $P = 0^d.70896 = \frac{1}{3} \times P_{orbit}$ and its first two harmonics are filtered from the data, the Fourier spectrum is reduced to noise consistent with the observational scatter (Fig. 8*b*). The Lafler-Kinman analysis also yields the same period. The resulting phase diagram is shown in Figure 9.

Are the perods found by the Fourier routine merely the harmonics of the orbital RV curve, indicating a nonsinusoidal shape and hence a nonzero eccentricity? The Fourier spectrum of an eccentric orbit would include the first harmonic at $\frac{1}{2} \times P_{orbit}$ as the largest secondary term, with consecutive harmonics ($\frac{1}{3}$, $\frac{1}{4}$, $\frac{1}{5}$, etc.) of monotonically decreasing amplitude. This is not what we find. In fact, the Fourier spectrum and the well-defined but nonsinusoidal residual curve are consistent with an *independent* secondary period P_2 and *its* first ($\frac{1}{2} \times P_2$) and second ($\frac{1}{3} \times P_2$) harmonics. Therefore, our result both confirms that the orbital eccentricity of CX Cep is indeed zero and reveals a coherent secondary variation which is one-third of the orbital period.

For the N IV λ4058 line, there is a forest of large residual peaks in the Fourier spectrum, but no simple pattern of frequencies and/or harmonics can be identified. Lafler-Kinman searches find no simple curves at any trial period. Finally, Fourier analysis of the N V λ4603 line shows no peaks which rise above the noise level.

The secondary period found in He II λ4686 cannot be explained by a desynchronization process as suggested by Marchenko (1988a) for other W-R binaries. Such processes do not necessarily lead to a simple period ratio like that seen here. It is more likely that this period is somehow related to the system's geometry. An asymmetry of the He II forming envelope and the presence of a bow shock (see § 3.4) might modify the observed RVs in a manner depending on orbital

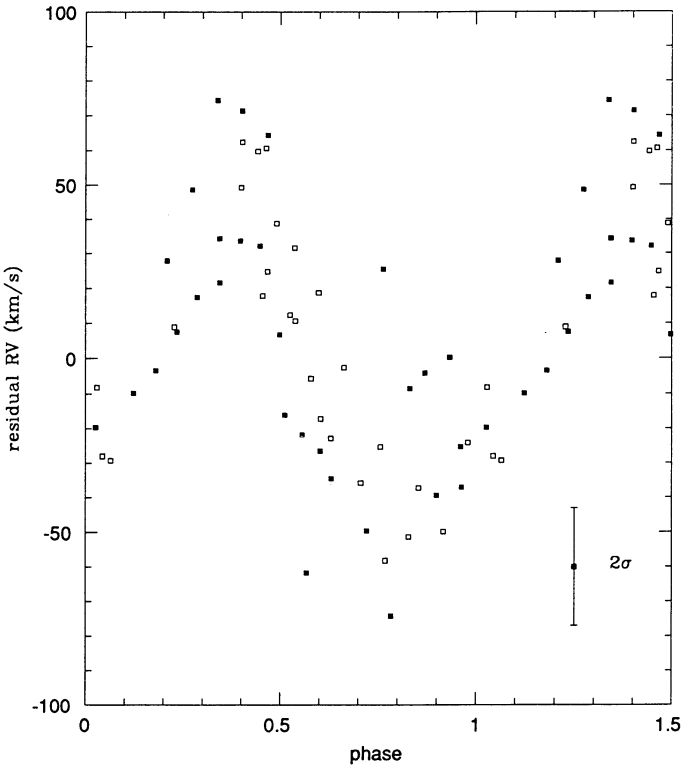

FIG. 9.—The velocity residuals analyzed in Fig. 7*a*, plotted at one-third of the orbital period of CX Cep and the same initial epoch as the orbital ephemeris. Symbols as in Fig. 3.

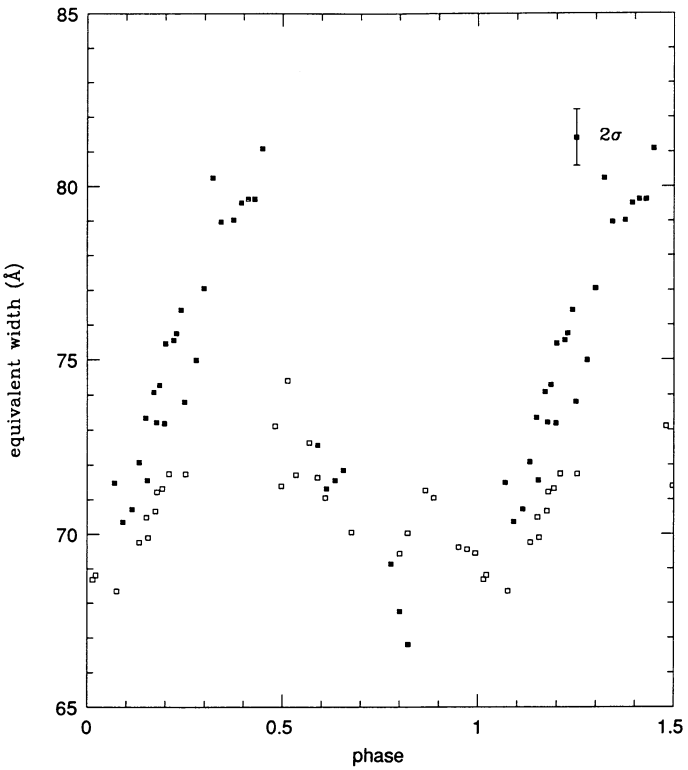

FIG. 10.—Equivalent width of the He II λ4686 emission line as a function of orbital phase. Symbols as in Fig. 3.

phase. This could explain why no clearcut variations are detected in the N IV and N V lines, since the line-emitting envelopes for these are expected to be more symmetric.

We note also that, for the He II and N IV lines searched, the amplitude of residual variations *increases* as the RV measurements are confined closer to the emission peak. This suggests that the mechanism responsible is operating at the line core. It may be the same process which produces the phase shifts described in § 3.2.3.

3.4. *Equivalent Width Variations: A Self-consistent Model of CX Cep*

We have studied the equivalent widths (EW) of the unblended emission lines N IV λ4058 and He II λ4686, of N V λ4603 and of the absorption component of the He I λ3888 P Cygni profile. The EWs of these lines are plotted against orbital phase in Figures 10–13. All reveal coherent variations with the orbital period.

Note the decrease in continuum intensity when the O star eclipses the core of the W-R star (at phase 0.5) should cause an apparent increase in the EW of the emission lines. However, since the dip in the continuum light curve at this eclipse is quite shallow (only ~0.03 mag), this effect is ~10 times smaller than the EW variations we observe. In the largely qualitative discussion which follows, this error can be safely neglected.

We interpret the variations of the individual lines in terms of the schematic model presented in Figure 14. This model assumes that the higher the ionization level, the closer to the W-R star is the corresponding line-forming envelope.[8] Table 5

[8] Other factors, such as the line intensity, can complicate the situation. For instance, the envelope of the very intense He II λ4686 line is larger than that of the less intense He II Pickering lines (Hillier 1987).

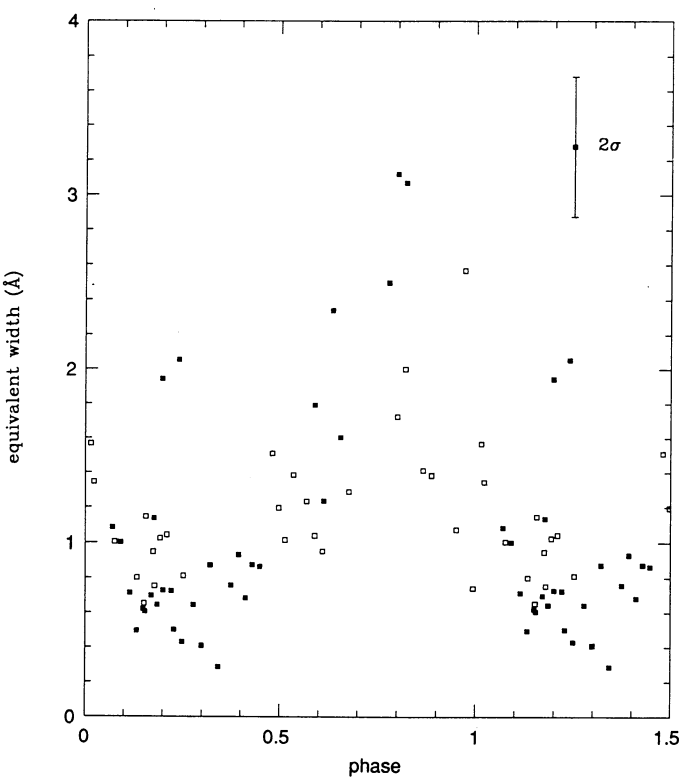

FIG. 11.—Equivalent width of the P Cygni absorption component of the He I λ3888 line as a function of orbital phase. Symbols as in Fig. 3.

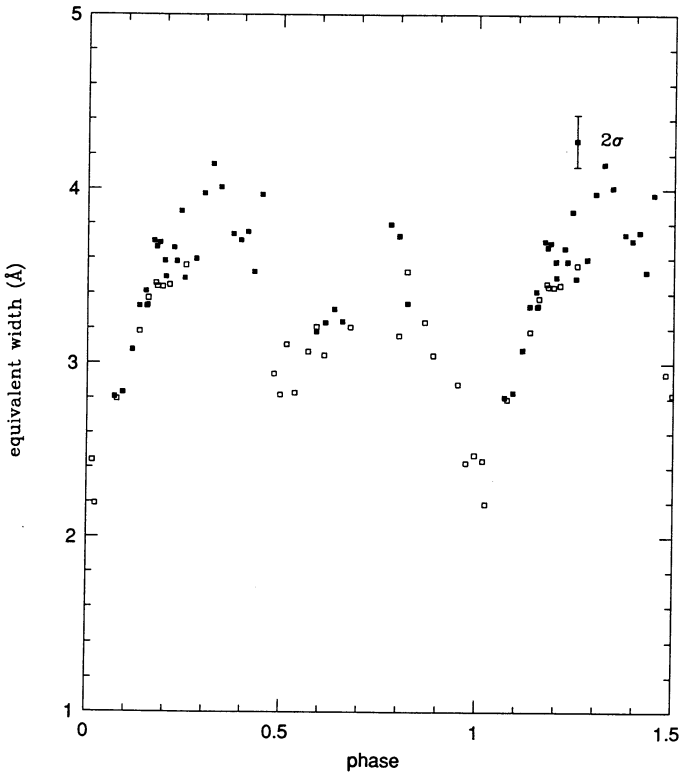

FIG. 12.—Equivalent width of the N v λ4603 emission as a function of orbital phase. Symbols as in Fig. 3.

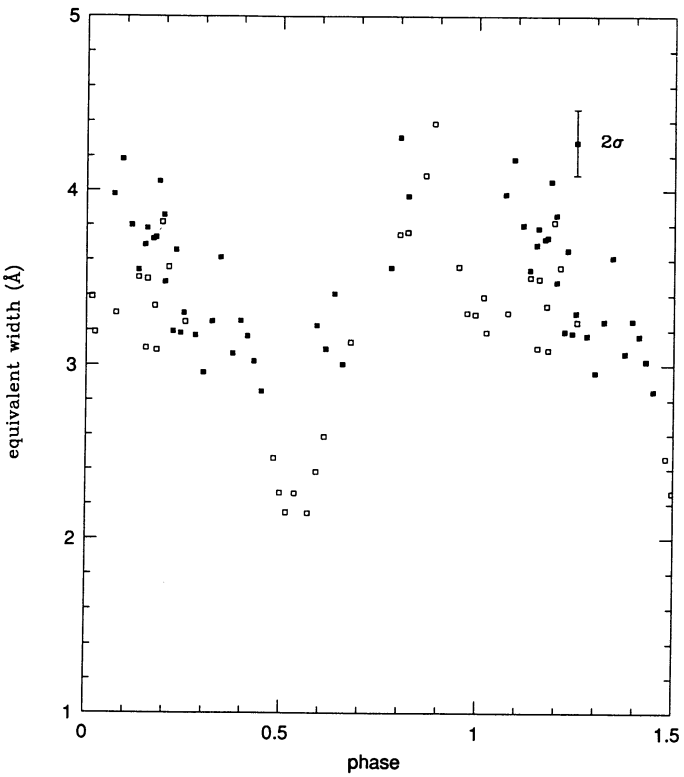

FIG. 13.—Equivalent width of the N IV λ4058 emission line as a function of orbital phase. Symbols as in Fig. 3.

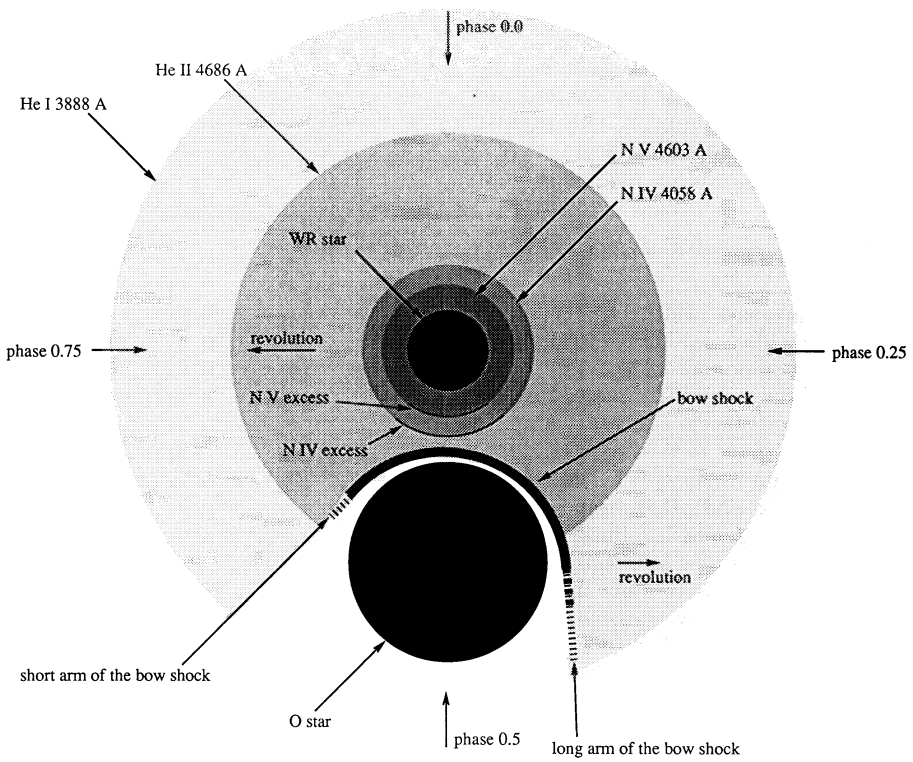

FIG. 14.—Sketch of the orbital plane of the binary CX Cep, in which the stars are drawn to scale based on the radii and separations derived in § 3.2.4. The stratification of line-forming regions in the W-R wind, and the wake and bow shock generated by the presence of the O star, are discussed in § 3.4. Note that the He I envelope actually extends far beyond the outer boundary shown.

TABLE 5

FORMATION REGIONS OF EMISSION LINES IN A WN5 STAR

Line	$r_{1/2}/R_\odot$
N IV λ4058	6–16
He II λ4686	10–50
He I λ3888	21–160
a_{orbit}(CX Cep)	25–32

NOTE.—The two values of $r_{1/2}$ are the radii corresponding to half-maximum intensity of line emission measured from the center of the WN5 star EZ CMa (Hillier 1985, 1987), assuming a core radius of $r_{core} = 2.5\ R_\odot$. Calculations of N V are not available.

shows the expected radii of line-forming regions in a WN5 wind (Hillier 1985, 1987) compared with our estimate of the orbital separation for CX Cep. N IV λ4058 and especially N V λ4603 are formed in smaller envelopes and should be sensitive only to conditions near the W-R stars. The He II λ4686 line is formed within a quasi-spherical envelope whose size is comparable to the distance between the two stars. It should be the most sensitive diagnostic of the overall behavior of the binary system. On the other hand, the metastable He I λ3888 emission occurs in a much larger envelope which encompasses the entire system and is thus less sensitive to changes within the envelope.

As depicted in Figure 14, the envelopes are interrupted by the "wake" of the O star within the W-R wind. There should be a bow shock at this interface which is longer at the leading edge of the O star in its orbit. Observing the system at different orbital phases gives us different views of the envelopes and this bow shock, which can explain the EW variations. It is important to remember in the subsequent discussion that this binary system is *not* viewed edge-on, so eclipses of the W-R star and its inner wind by the O star are only partial. We discuss the model in greater detail—line by line—in the following subsections.

3.4.1. He II λ4686

As with the average RVs, there appears to be a systematic difference in the flux of this line between the two runs. The shift of ~2%–3% is, however, much smaller than the ~15% variation with orbital phase seen in Figure 10.

The shape of the EW curve is somewhat unusual. The line flux increases between phases 0.0 and 0.4, followed by a sharp drop which becomes more gradual until reaching a minimum near phase 0.8. Between phase 0.8 and 0.9, there appears to be a difference in the EW variation between the runs which is in the opposite sense to the systematic shift noted above. The different trends in this phase interval depend heavily on only a few points, but if taken at face value, the largest discrepancy is at the 4 σ level. It is possible that the He II λ4686 emitting region has changed in the 2 months between the observing runs. We address this possibility below. Also keep in mind that this line has the highest S/N in our spectra, and because its line-forming region is comparable in size to the binary separation, it should be the most sensitive to long-term changes in the wind and/or binary parameters.

The general behavior of the EW curve in Figure 10 can be explained by the model in Figure 14, in which we propose an excess of He II λ4686 in the long arm of the bow shock, where the O star is "ploughing" through the W-R wind. The excess is due to shock heating, and results in a higher level of ionization. The increase in EW from phase 0.0 to 0.4 is a result of seeing the bow shock through a diminishing amount of absorbing wind material. Since the shock front is very close to the O star, it is rapidly eclipsed near phase 0.5, and it most completely hidden near phase 0.8. Marchenko (1988b) estimated that the total contribution to the He II λ4686 flux from the bow shock region of the W-R binary V444 Cyg is ~5%. Allowing for the stronger stellar wind from an O5 star (compared to the O6 star in V444 Cyg) and the smaller separation of the components in CX Cep, stronger wind-wind interactions—and hence larger He II variation (~15%)—are not unexpected.

It is at this point that we note the possible difference in EW behavior between the two runs. During the first run, the excess in He II due to the bow shock may have become visible earlier. In the geometry of Figure 14, this could be explained by (1) a change in the W-R wind density, reducing the optical depth of the inner obscuring wind, and/or (2) a transient increase in the strength and extent of the bow shock. It is unlikely that there was a change in the radius and overall density of the W-R wind during the 2 month interval, since the spectral type of the W-R star remained the same in spectra from the two runs. However, a local change in wind density along the line of sight at phases 0.8–0.9 could be caused by the presence of blobs in the wind. Since blobs have been inferred in other W-R winds by Moffat et al. (1988). These same blobs could also cause perturbations which are felt most strongly in the bow shock. In this way, the He II λ4686 emitted at that front could show a nonlinear response to the wind variations.

3.4.2. He I λ3888 *P Cygni Profile*

The absorption component of this profile shows a maximum near phase 0.8 and a minimum near phase 0.3 (see Fig. 11) but there is too much scatter to discern any details about the shape of the EW curve. Nevertheless, its general form (particularly the anticorrelation with the He II curve of Fig. 10) can be understood in the context of our model.

As seen in Figure 14, at phases near 0.8, the largest column densities of He I are projected in front of *both* the W-R and O star, resulting in maximum He I absorption. At this phase, the bow shock is effectively hidden, so the He II emission is at a minimum. In contrast, near phases 0.4–0.5, the amount of He I which contributes to absorption is near its minimum, because the O star is in the foreground of the envelope and much of the He I is absent in that star's wake. Enhancing this effect is the fact that the intense ionization region of the bow shock is closest to the observer near phase 0.3, diminishing the supply of neutral He I λ3888. This is also the phase where the He II emission is near maximum because that part of the bow shock is viewed through the smallest amount of intervening gas.

3.4.3. N V λ4603

Figure 12 shows that the equivalent width of this line has two unequal minima, at phases 0.0 (W-R star in front) and 0.5 (O star in front). This suggests that a nonnegligible amount of N V is formed between the two stars. As noted at the beginning of § 3.4, this high-ionization line is formed mainly in a thin envelope centered on the W-R star and is less prone to gravitational distortions of the companion than, say He II λ4686. However, the asymmetry of the EW curve in Figure 12 points to an excess of emission on the side of the W-R envelope which faces its companion. This is probably due to heating from the O star, which produces an increase in ionization and, hence, in N V emission strength.

3.4.4. N v λ4058

The equivalent width of this line also undergoes local minima near phases 0.0 and 0.5 (see Fig. 13), but the relative depths are opposite in sense to those of the N v λ4603 curve. Like the N v line, N IV is formed in an envelope centered on the W-R star, but slightly more extensive. There should also be an excess of emission of N IV on the side of the envelope facing the O star, as we argued for N v. However, this will occur farther from the W-R star and so the surface of excess N IV emission is more extended. For this reason, we expect the N IV line to be weakened less by the eclipse at phase 0.0. On the other hand, at phase 0.5 when the N IV and N v envelopes are partially eclipsed by the O star, more of the N IV excess region is hidden because it forms closer to the O star than the N v excess.

3.5. *Line Asymmetries*

Emission lines were tested for asymmetry by searching for a systematic change in their radial velocities measured upward from different levels above the continuum. If this indicated an asymmetry, then a skewness analysis was performed to quantify its behavior with phase.

In the case of He II λ4686, the montage of profiles in Figure 15 clearly demonstrates varying line asymmetry. The skewness is shown as a function of orbital phase in Figure 16. The radial velocity measured from this skewed line is strongly dependent on level, as shown in Figure 17. Above ~50% of the line height, the derived RV amplitude ($K \sim 340$–350 km s^{-1}) is roughly constant within the errors. (It is at these levels that the RV orbital solution was obtained.) For comparison, the

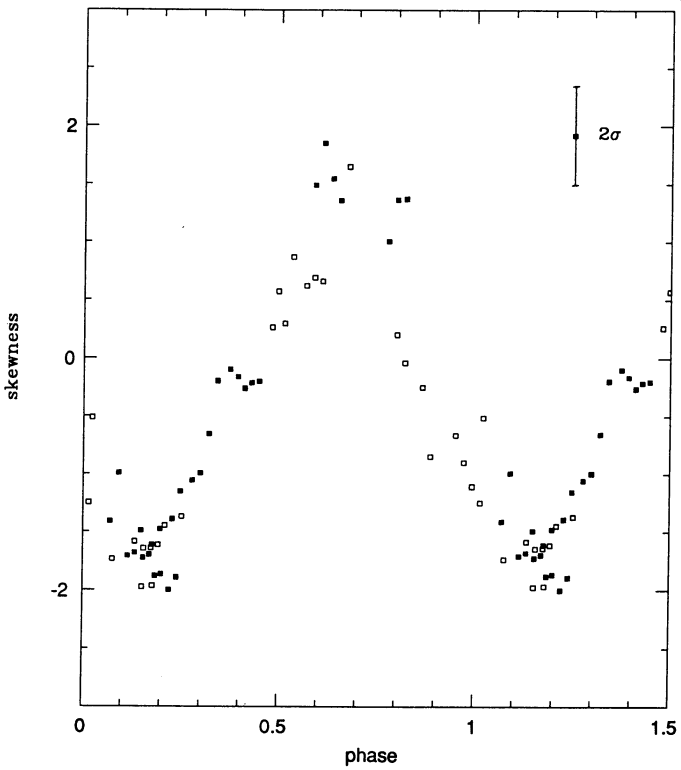

FIG. 16.—The skewness of the He II λ4686 profiles as a function of orbital phase. Symbols as in Fig. 3.

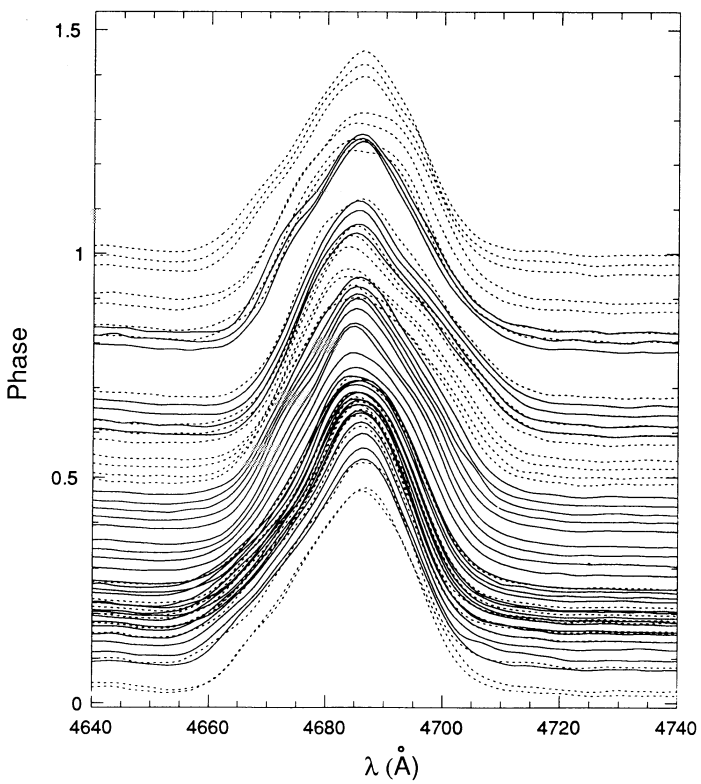

FIG. 15.—A montage of the individual He II λ4686 profiles, shifted by the adopted emission-line orbital fit to the same radial velocity and ordered according to orbital phase. Dashed profiles are the 1987 August data; solid profiles are the 1987 October data.

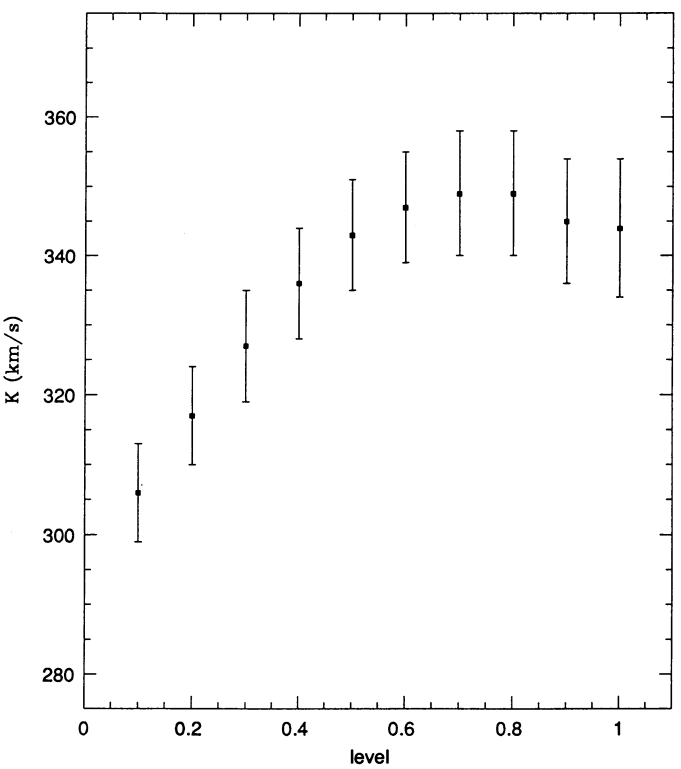

FIG. 17.—Variation of the RV amplitude of the He II λ4686 line as a function of the level of the profile above which the velocity is measured.

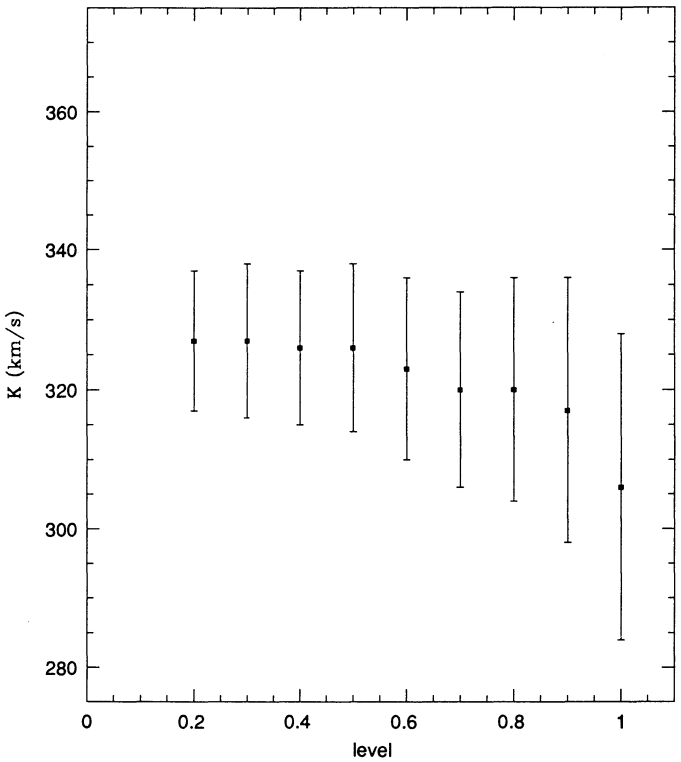

FIG. 18.—Same as Fig. 16, but for N IV λ4058

derived K value of the N IV λ4058 line does not vary significantly with level (Fig. 18), consistent with no changes in profile symmetry during the orbit.

In our model, N IV λ4058 is formed in a quasi-spherical envelope. The wind expansion velocity at the surface of this envelope should be nearly radial, so we would expect this line to be symmetric. Since the wake of the O star cuts out a large portion of the He II λ4686 envelope, pronounced asymmetries are introduced in this line. Near phase 0.0, there is less He II expanding away from the observer, so the redshifted component of the line is reduced; near phase 0.5, the blueshifted component is smaller. If the O-star wake were pointed directly away from the W-R star, then the extrema in asymmetry would occur *exactly* at phases 0.0 and 0.5. However, since the wake slightly trails the orbital path of the O star (see Fig. 14), these extrema should lag these phases by a small amount. This is in fact what we observe in Figure 16.

4. SUMMARY

CX Cep is the W-R + O binary with the second-shortest period known in the Galaxy, after CQ Cep ($P = 1^d.64$). Its components appear similar to the well-known eclipsing binary V444 Cyg (WN5 + O6 V; $P = 4^d.2$), for which modern spectroscopic data in the blue are still lacking.

Our study of CX Cep has uncovered the following new results:

1. We confirm that the W-R component is of type WN 5, but we find that the companion is an O5 V star, rather than O8 V as suggested previously.
2. The radial velocity orbit (best defined by the N V λ4603 emission line for the W-R star and the photospheric Balmer absorption lines for the O star) is consistent with the photometric period of $2^d.12687$.
3. The orbital eccentricity is near zero.
4. The individual masses can be obtained from $M_O \sin^3 i = 25.2 \pm 1.9\ M_\odot$ and $M_{WR} \sin^3 i = 17.8 \pm 1.4\ M_\odot$, but it is still not clear whether $i = 74°$ (based on polarimetry) or $i = 50°$ (according to light curve analyses and spectroscopic estimates of the O-star masses).
5. Despite its short period, CX Cep is not a contact binary system.
6. There is a secondary RV variation in the He II λ4686 line with a period of exactly one-third of the orbital period. This is not a simple harmonic indicating orbital eccentricity but an independent variation with its own harmonics. This may represent a subtle distortion of the He II forming envelope around the W-R star by the O companion.
7. Phase-dependent equivalent width variations are observed in He II λ4686 emission, He I λ3888 P Cygni absorption, and the N IV λ4058 and N V λ4603 emission lines.
8. Phase-dependent line asymmetries occur in the He II λ4686 line, while N IV λ4058 appears to be symmetric.
9. The EW and asymmetry variations can be explained by a qualitative model (shown in Fig. 14) in which lines of higher ionization are formed in concentric envelopes of the wind closer to the W-R star. Within the wind, the O-type companion creates both a wake and a bow shock where excess He II emission occurs. N IV and N V excess emission is due to heating of the W-R wind by the O star. The He I absorption variations are mainly due to the hole left in the He I envelope by the O star's wake. Similarly, the profile asymmetries of He II are caused by the intersection of the O star with the He II–emitting envelope. N IV is formed close enough to the W-R star that the presence of the O star does not significantly distort the quasi-spherical symmetry of its envelope.

We are grateful to NSERC (Canada) and FCAR (Québec) for financial assistance. We would also like to thank Laurent Drissen for kindly obtaining some of the first spectra used in this work.

REFERENCES

Abbott, D. C., & Conti, P. S. 1987, ARA&A, 25, 133
Aspin, C., Simmons, J. F. L., & Brown, J. C. 1981, ApJ, 194, 283
Bracher, K. 1966, Ph.D. thesis, Indiana University
Deeming, T. J. 1975, Ap&SS, 36, 137
Drissen, L., Lamontagne, R., Moffat, A. F. J., Bastien, P., & Seguin, M. 1986, ApJ, 304, 188
Harmanec, P. 1988, Bull. Astron. Inst. Czechoslovakia, 39, 329
Hillier, D. J. 1985, in Luminous Stars and Associations in Galaxies, ed. C. W. H. de Loore, A. J. Willis, & P. Laskanides (Dordrecht: Reidel), 261
———. 1987, ApJS, 63, 965
Hiltner, W. A. 1946, PASP, 58, 215
———. 1948, ApJ, 108, 56
Howarth, I. D., & Prinja, R. K. 1989, ApJS, 69, 527
Kurtz, D. W. 1985, MNRAS, 213, 773
Lafler, J., & Kinman, T. D. 1965, ApJS, 11, 216
Lewis, D. 1991, M.Sc. thesis, Université de Montréal
Lipunova, N. A., & Cherepashchuk, A. M. 1982, AZh, 59, 73
Marchenko, S. V. 1988a, Pisma Astron. Zh., 47, 248
———. 1988b, Kinemat. Phys. Celest. Bodies, 4, No. 6, 36
Massey, P. 1981, ApJ, 246, 153
Massey, P., & Conti, P. S. 1981, ApJ, 244, 169
Mathys, G. 1988, A&AS, 76, 427
———. 1989, A&AS, 81, 237
Matthews, J. M., & Wehlau, W. H. 1985, PASP, 97, 841

Moffat, A. F. J., Drissen, L., Lamontagne, R., & Robert, C. 1988, ApJ, 334, 1038
Moffat, A. F. J., Lamontagne, R., Shara, M. M., & McAlister, H. A. 1986, AJ, 91, 1392
Prinja, R. K., Barlow, M. J., & Howarth, I. D. 1990, ApJ, 361, 607
Robert, C. 1992, Ph.D. thesis, Université de Montréal
Scargle, J. D. 1982, ApJ, 263, 835
Schmidt-Kaler, Th. 1982, in Numerical Data and Functional Relationships in Science and Technology, Group 6, Vol. 2b, ed. K. Schaiffers & H. H. Voigt (Berlin: Springer), 1
Schulte-Ledbeck, R. E., & van der Hucht, K. A. 1989, ApJ, 337, 872
Svechnikov, M. A. 1969, Uch. Zap. Ural. Gos. Univ., 88, 134
Tassoul, J.-L. 1987, ApJ, 322, 856
Tassoul, J.-L. 1989, ApJ, 324, L71
———. 1990, ApJ, 358, 196
van der Hucht, K. A. 1991, in Wolf-Rayet Stars and Interrelations with Other Massive Stars in Galaxies, ed. K. A. van der Hucht & B. Hidayat (Dordrecht, Kluwer), 19
van der Hucht, K. A., Conti, P. S., Lundström, I., & Stenholm, B. 1981, Space Sci. Rev., 28, 227
van der Hucht, K. A., Hidayat, B., Admiranto, A. G., Supelli, K. R., & Doom, C. 1988, A&A, 199, 217
Vreux, J.-M. 1985, PASP, 97, 274
Vreux, J.-M., Andrillat, Y., & Gosset, E. 1985, A&A, 149, 337
Vyssotsky, A. N., Miller, W. J., & Walther, M. E. 1945, PASP, 57, 314